ACS Photonics

pubs.acs.org/journal/apchd5

Article

Fully Suspended MoS_2 Photodetectors toward High Response Speed and Stable Responsivity

Jianyong Wei,[⊥] Zhentao Lian,[⊥] Yumeng Liu, Maosong Xie, Yueyang Jia, Kai Li, Robert Kudrawiec, Yaping Dan,* and Rui Yang*

Cite This: *ACS Photonics* 2025, 12, 2656−2663

Read Online

ACCESS | Metrics & More | Article Recommendations | Supporting Information

ABSTRACT: High photoresponsivity has been achieved in photodetectors based on two-dimensional (2D) semiconductors, but they usually suffer from low response speed and severe responsivity decay with higher light intensity due to substrate effects. In this work, photodetectors with high response speed and stable responsivity are prepared based on fully suspended MoS_2. Due to the complete separation of the suspended MoS_2 channel and the Si substrate underneath, the photogating effect is effectively suppressed. Then the photocurrent rise and fall times are measured as 68.6 and 100.0 μs by transient photocurrent measurement, respectively, which are about 10^5 times faster than the nonsuspended devices. Moreover, they exhibit stable responsivity with time within a large range of light intensity. A detailed analysis of the photoresponse mechanisms is performed by comparing the photoresponses from devices with different structures. The results provide a fundamental understanding of photoresponse mechanisms and guide the design of high-performance 2D photodetectors.

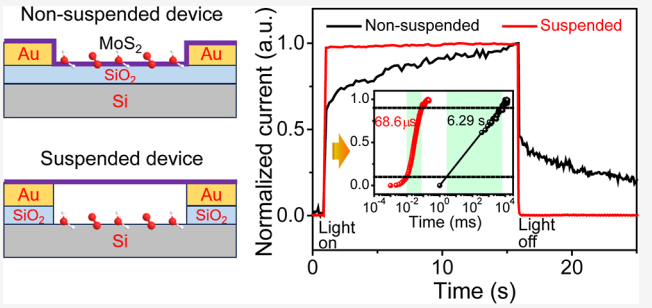

KEYWORDS: *suspended photodetector, 2D phototransistors, response speed, MoS_2, transient response, photoresponse mechanism, interface effect*

INTRODUCTION

During the past decade, two-dimensional (2D) semiconducting transition metal dichalcogenides (TMDCs) have been extensively investigated and seen as potential candidates for next-generation electronic and optoelectronic devices due to their unique optical and electrical properties,[1−3] such as atomic-scale thickness, high carrier mobility, tunable bandgap, as well as wafer-scale integration capability.[4,5] Among the various TMDCs, 2D molybdenum disulfide (MoS_2) attracts lots of attention for its thickness-dependent bandgap, relatively high electron mobility over 200 $cm^2/(V\ S)$, and high optical absorption.[6] Phototransistors can be fabricated by simply constructing 2D transistors employing monolayer or multilayer MoS_2 as channel material under light irradiation.[7−9] As reported, phototransistors based on pure MoS_2 channel can achieve ultrahigh responsivity of 880 (monolayer) and 4.3×10^3 A/W (multilayer).[10] Moreover, van der Waals heterostructures can further improve the responsivity of 2D phototransistors.[11−13] The responsivity of phototransistors based on multilayer MoS_2 can be even improved to 6.0×10^3 A/W by building van der Waals heterostructures between zero-dimensional (0D) silicon quantum dots and 2D MoS_2.[14]

Although MoS_2-based phototransistors have achieved excellent responsivity and detectivity, there are still some problems to be solved. One is the low response speed to light. MoS_2-based phototransistors usually take several seconds to achieve a saturated current under light illumination,[2,7,15−17] which is far from the practical need. Although photogating effect due to the trap states can enhance the photoresponsivity, it also limits the speed.[18,19] While some techniques such as h-BN encapsulation have been explored to improve the interface, the trap effect from the underlying substrate has not been fully eliminated.[20−22] Another problem is the severe responsivity decay with the increasing incident light intensity,[2,7] which is due to the complex carrier generation, trapping, and recombination processes within the 2D semiconductors.[18]

To address these problems, in this work, we design a new photodetector with a fully suspended MoS_2 channel to separate the MoS_2 channel and Si back gate. The suspended structure effectively suppresses the trap-state-induced photogating effect and simplifies the dynamic process of carrier transport. As a result, the photocurrent rise time and fall time are measured as 68.6 and 100.0 μs by transient photocurrent measurement, respectively, which are about 10^5 times faster than the nonsuspended phototransistors. Moreover, the responsivity of

Received: January 16, 2025
Revised: April 16, 2025
Accepted: April 18, 2025
Published: April 24, 2025

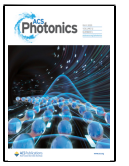

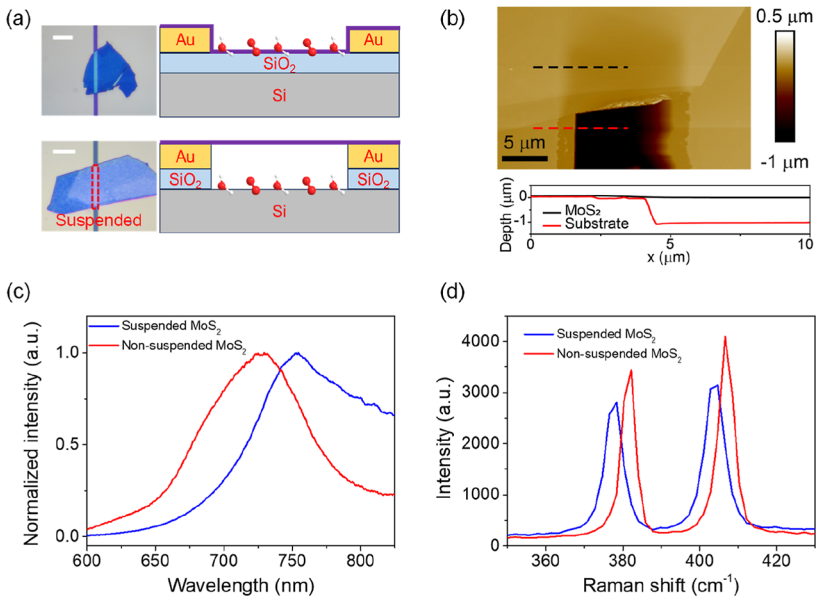

Figure 1. (a) Optical images and schematic diagrams of nonsuspended (top) and suspended (bottom) MoS_2 devices. The scale bar is 20 μm. (b) AFM image of a suspended MoS_2 device, with the line scan along the black and red dashed lines shown on the bottom. (c) Photoluminescence spectra and (d) Raman shifts of the suspended and nonsuspended MoS_2.

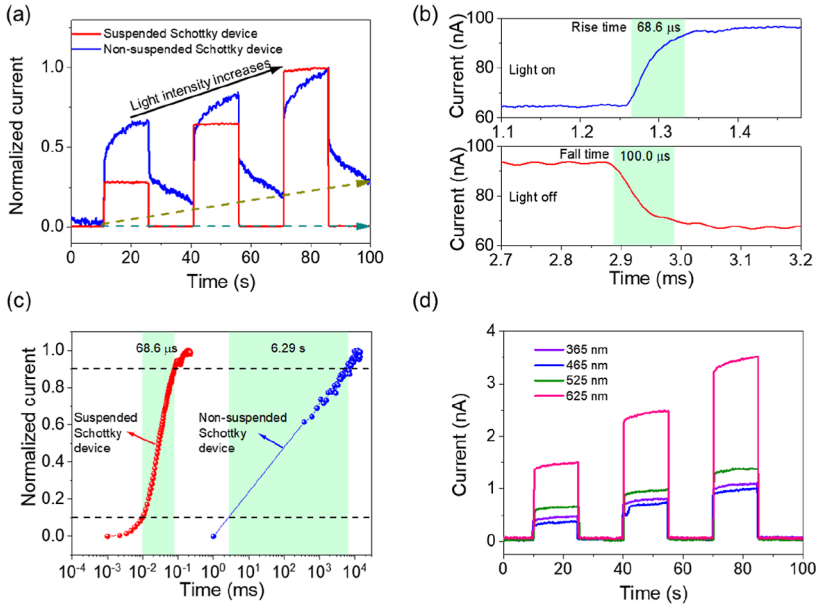

Figure 2. (a) Normalized current of the nonsuspended and suspended Schottky-contact devices under increased light illumination over time, as shown by the black arrow. (b) Transient measurements showing the current rise and fall processes of the suspended device when the light turns on or off. (c) Summary of the photocurrent rise time of the suspended and nonsuspended devices. (d) Current of the suspended device under different wavelengths of light illumination with increased intensity over time.

suspended device remains stable within a wide range of light intensity. Furthermore, according to the comparison of photoresponses of MoS_2-based photodetectors with different structures, a detailed analysis of the photoresponse mechanisms has been performed. This work provides fundamental guidance for the design of 2D photodetectors with high performance.

RESULTS AND DISCUSSION

The slow speed of light response and decay of responsivity with light intensity have become obstacles for the further development of MoS_2-photodetectors, which is mainly related to the dangling bonds or slow traps on the surface of the oxide underneath. Therefore, to avoid such influence on the MoS_2 channel and improve the light response speed, we design photodetectors with a fully suspended MoS_2 channel and compare them with the normal nonsuspended MoS_2 devices. The optical images and schematic diagrams of the nonsuspended (on the top) and suspended (on the bottom) MoS_2 field effect transistors are shown in Figure 1a, with both MoS_2 flakes in contact with and on top of the Au electrodes. The nonsuspended devices are fabricated by lithographically patterning the Au/Cr electrodes on the p^+-Si/300 nm SiO_2 wafer, followed by mechanical exfoliation and dry-transfer of

https://doi.org/10.1021/acsphotonics.5c00146
ACS Photonics 2025, 12, 2656−2663

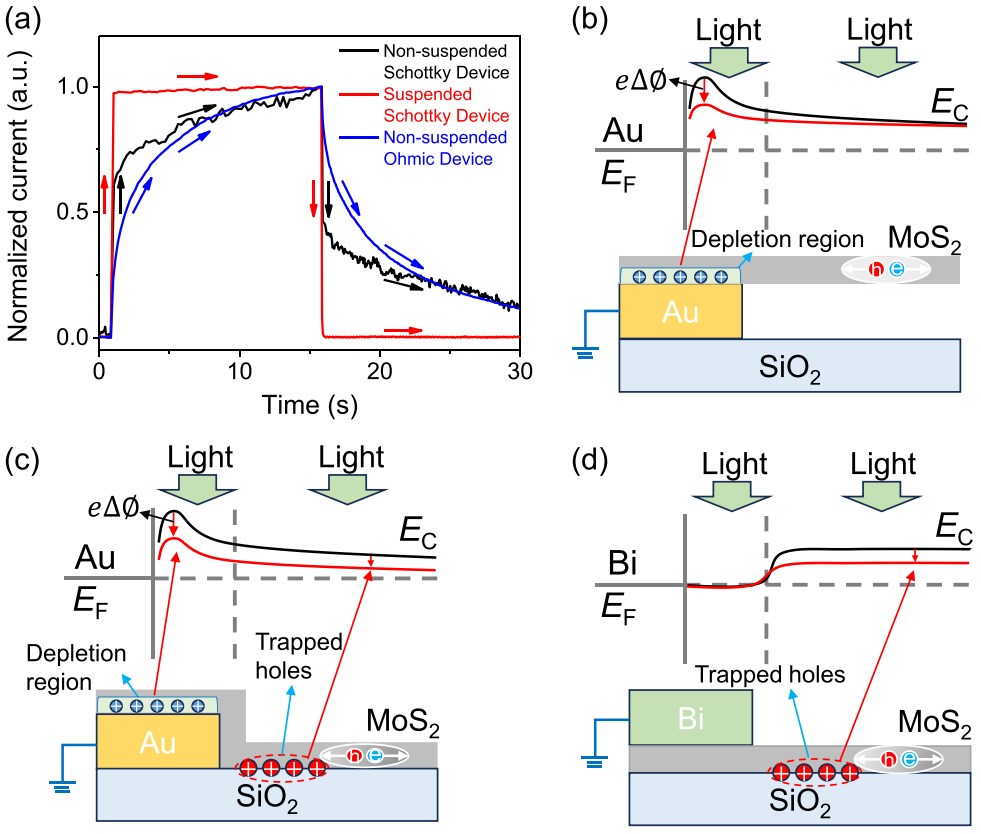

Figure 3. (a) Comparison of normalized current of a suspended Schottky-contact device, nonsuspended Schottky-contact device, and nonsuspended Ohmic-contact device. Schematic energy band structure and device structure of the (b) suspended Schottky-contact device, (c) nonsuspended Schottky-contact device, and (d) nonsuspended Ohmic-contact device under light illumination.

MoS_2.[23] To achieve complete separation of the Si substrate and the MoS_2 channel, the fabrication procedures of the substrate with suspended MoS_2 are modified. Au/Cr metals are first evaporated on the p^+-Si/300 nm SiO_2 wafer without photolithography, so that the metal film covers the full surface of the wafer. Then the surface microtrench is formed by photolithography and reactive ion etching of the Au/Cr, SiO_2, and Si in the channel area, leaving a ∼1 μm deep microtrench. Then a MoS_2 flake is mechanically exfoliated and dry-transferred onto the microtrench, forming the suspended MoS_2 channel. For both suspended and nonsuspended MoS_2, the channels are ∼10 μm long.

To make sure the MoS_2 channel is fully suspended, the atomic force microscopy (AFM) characterization is conducted and the image is shown in Figure 1b. The black line and red line show the depth of the MoS_2 and blank channel along with the horizontal x axis direction, which shows that the channel depth is about 1 μm and the MoS_2 channel is suspended as a flat membrane over the microtrench and separated from the substrate. The MoS_2 quality of the two devices is examined with photoluminescence (PL) and Raman spectroscopy. The slight red-shift of the suspended MoS_2 compared with the nonsuspended MoS_2 indicates tensile strain after the suspension (Figure 1c). As shown in Figure 1d, the E^1_{2g} and A_{1g} Raman peaks also show red-shift for the suspended MoS_2 (378.4 and 404.7 cm^{-1}) compared with the nonsuspended device (382.2 and 406.6 cm^{-1}), further confirming the tensile strain in the suspended MoS_2. The frequency differences of the two devices are 26.3 and 24.4 cm^{-1}, which shows the two MoS_2 flakes are more than six layers.[24]

Then the electrical properties of the two devices are explored. Figure S1a shows the I_d−V_{ds} curves of the suspended (blue) and nonsuspended (red) devices, both of which exhibit obvious nonlinearity. This behavior is quite common for 2D transistors with Schottky junctions between Au and 2D semiconductors, which is mainly caused by Fermi level pinning effect,[25−27] and strain between metal and 2D semiconductors.[28,29] Transfer characteristics of the two devices are plotted in Figure S1b. The suspended device shows smaller on/off ratio than the nonsuspended device, which might be related to the thicker dielectric layer or varied contact condition. Then the optoelectronic properties of the two devices over a long time scale are studied under the illumination of a commercial 525 nm LED. As shown in Figure 2a, both devices have a strong response to light. For the nonsuspended device, when the light is turned on, the current experiences an abrupt jump and then begins to slowly increase. The rise time, which is defined by the time needed to increase from 10% to 90% of the maximum current, is extracted as ∼6 s from the light response curve for the nonsuspended device. By comparison, the current of the suspended device only experiences an abrupt increase after the light is turned on and then reaches saturation. Obviously, the suspended device shows a much faster response speed compared to the nonsuspended device, which agrees well with our expectation. Moreover, after the light is turned off, the current of the suspended device can rapidly drop back to its initial value while the current of the nonsuspended device remains at a much higher value than the initial value and gradually decreases. As the light intensity (P_{light}) increases, the dark current of the nonsuspended device keeps increasing

https://doi.org/10.1021/acsphotonics.5c00146
ACS Photonics 2025, 12, 2656−2663

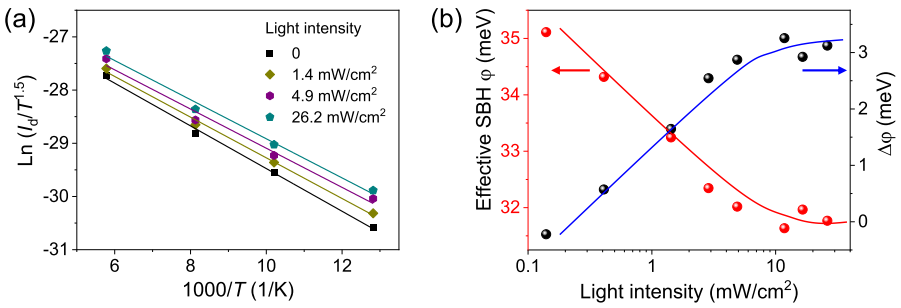

Figure 4. (a) Arrhenius plots of the suspended MoS_2 device under light illumination (λ = 525 nm) of different intensities. (b) Effective SBHs and SBH reduction as a function of light intensity.

while that of the suspended device can always drop back to the baseline of dark current.

To obtain the specific light response time of the suspended device, transient photocurrent measurements within the short time scale are carried out with a 405 nm pulsed laser with a rise and fall time less than 3 ns, and the transient current rising and falling processes are shown in Figure 2b. The rise and fall time are extracted as 68.6 and 100.0 μs. Then the rising process of the two devices is plotted in Figure 2c, which shows the rise time of suspended device is reduced by about 5 orders of magnitude compared to the nonsuspended device. To further determine the fast response of the suspended device, the photoresponse cutoff frequency has been measured. As shown in Figure S2, the cutoff frequency at −3 dB is about 64 kHz, indicating an ultrafast response speed. Then the responses to light with long time scale at different wavelengths for the suspended device are measured using four LEDs (365, 465, 525, and 625 nm). As shown in Figure 2d, no matter which wavelength of LED is used, the suspended device exhibits ultrafast response speed. Moreover, the device shows the strongest response to the 625 nm light, which shows that the device has the highest quantum efficiency under 625 nm light illumination.

According to the results above, when the suspended device is exposed to light, its current will undergo a rapid increase in tens of microseconds and then reach saturation, where there is only a rapid current rising process, as shown in Figure 3a. Similarly, when the light is turned off, there is only a rapid current falling process. In contrast, for the nonsuspended device, when the light is turned on, its current will undergo a rapid increase and then a slow increase on the time scale of a few seconds. The situation when light is turned off is similar. From previous models, the photocurrent of the phototransistors can be mainly generated from the photoconductive effect, photogating effect, and photoinduced Schottky barrier reduction.[30−32] The photoconductive effect directly generates photocurrent in the device channel, the photogating effect mainly occurs at the interface between the MoS_2 channel and SiO_2 substrate, and the photoinduced Schottky barrier reduction occurs in the contact area of the MoS_2 and metal electrodes. Since the MoS_2 in the suspended device is fully separated from the SiO_2 substrate, the photogating effect is suppressed in this case. Therefore, the results suggest that the photocurrent generation in the channel (by the photogating effect and photoconductive effect) is a slow process due to trap states (on the time scale of seconds), while the photocurrent generation by photoinduced Schottky barrier reduction is a fast process (on the time scale of microseconds).

To further validate the hypothesis, a device with Ohmic contact is fabricated by using Bi as the contact layer. The rigidly linear $I-V$ curve (Figure S3) shows this device has a desirable Ohmic contact. When the light is turned on, the current begins to grow slowly, and it takes several tens of seconds to saturate (Figure 3a). Compared with the suspended device and the nonsuspended Schottky-contact device, the nonsuspended Ohmic-contact device only has a slow photocurrent rising process. When the light is turned off, the current also only undergoes a slow falling process. The photocurrent of the nonsuspended Ohmic-contact device mainly comes from the photogating effect in the channel because there is no Schottky barrier. Therefore, the results are consistent with the hypothesis above.

To better understand the photoresponse mechanisms of these three types of devices, the schematic energy band diagram and device structure of the suspended Schottky-contact device, nonsuspended Schottky-contact device, and nonsuspended Ohmic-contact device under light illumination are shown in Figure 3b−d, respectively. For the suspended device, due to the Schottky junction formed at the contact area between MoS_2 and Au, its current is governed by a dual-Schottky-junction model.[33] When the device is under light illumination, photogenerated electron−hole pairs will narrow the depletion region in the MoS_2 side and reduce the Schottky barrier height. As the Schottky barrier is reduced, device current can be improved according to the dual-Schottky junction model, which is the origin of the photocurrent and exhibits a fast response speed.

For the nonsuspended Schottky-contact device, its current is also governed by the dual-Schottky-junction model due to the Au−MoS_2 contact. Similarly, this device also undergoes a fast reduction of the Schottky barrier under light illumination. Besides, the photogating effect plays a role at the same time, and the photogenerated holes are trapped by the impurities on the oxide surface and distribute spatially in the channel, which forms an additional electric field just like the effect of gate voltage, and enhances the channel conductance. Due to the prolonged excess carrier lifetime and the gradual accumulation of hole trapping, the conductance modulation by the photogating process is a slow process. For the nonsuspended Ohmic-contact device, the conduction energy band of MoS_2 is below its Fermi level near the Bi electrode, resulting in a negligible Schottky barrier. Therefore, there is only a photogating effect under light illumination, which will slowly enhance the channel conductance. These mechanisms can well explain the dynamic photoresponse of different types of MoS_2-based photodetectors.

https://doi.org/10.1021/acsphotonics.5c00146
ACS Photonics 2025, 12, 2656−2663

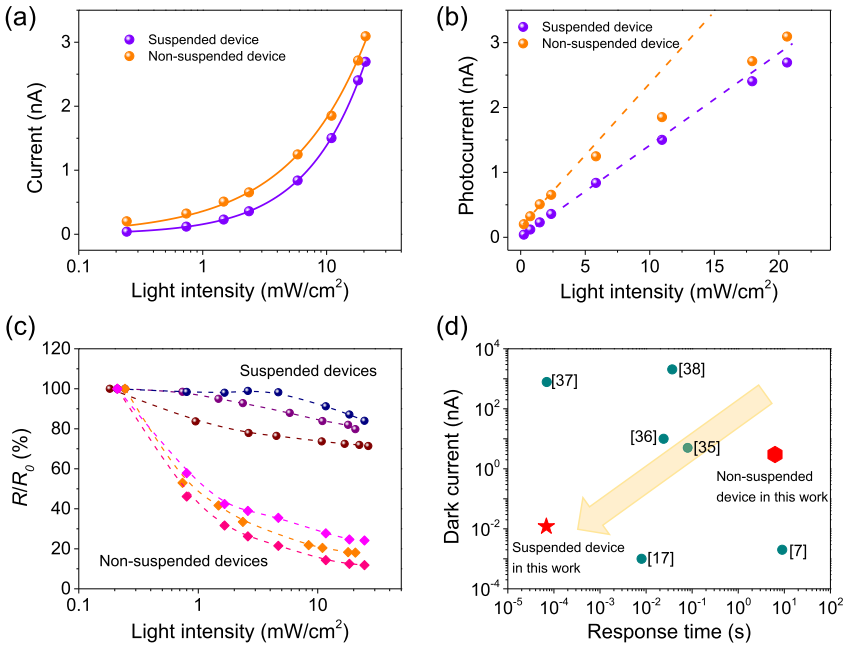

Figure 5. (a) Total current of the suspended and nonsuspended MoS_2 devices under light illumination dependent on light intensity (P_{light}) and fitting results with eq 2. (b) Photocurrent ($I_{ph} = I_{illum} - I_{dark}$, I_{illum} is the device current under light illumination and I_{dark} is the dark current) of the suspended and nonsuspended MoS_2 devices dependent on light intensity. The dashed linear lines are guides to the eye. (c) The photoresponsivity changes of the device as light intensity increases. (d) A summary of the response time and dark current of the photodetectors based on a pure MoS_2 channel in literature.

To further validate the photoresponse mechanism of the fully suspended device, temperature-dependent photoresponse measurements are carried out and the light-intensity-dependent Arrhenius plots ($\ln(I_{ds}/T^{1.5})$ *vs.* $1000/T$) are shown in Figure 4a. The Arrhenius plots with negative slopes confirm that the device has a Schottky contact. As the light intensity increases, the slope gradually increases, showing a gradually decreasing Schottky barrier height. Then the Schottky barrier height and its reduction are extracted and plotted as a function of the light intensity in Figure 4b. As the light intensity increases from 0 to 26.2 mW/cm^2, the Schottky barrier height gradually decreases from 34.9 to 31.8 meV. These results are well consistent with the hypothesis above.

Previously, a photoresponse model based on Schottky-contact MoS_2 phototransistors has been established.[33] According to this model, the relationship between P_{light} and Schottky barrier reduction $\Delta\phi$ has been written as

$$P_{light} = P_{light}^{S}\left[\exp\left(\frac{\Delta\phi}{mkT}\right) - 1\right] \quad (1)$$

where P_{light}^{S} is defined as the critical light intensity given by $P_{light}^{S} = \frac{\hbar\omega n_i}{2\alpha\tau_0}$, in which $\hbar\omega$ is the photon energy, n_i is the intrinsic electron concentration (per unit area) of MoS_2, α is the light absorption ratio by MoS_2, and τ_0 is the minority carrier recombination lifetime in MoS_2. M is the ideality factor determining how effectively the potential barrier is reduced by light illumination, which depends on the device structure, light absorption, defects in the junction, *etc.* The total current I_{illum} is related with the light intensity P_{light} as follows

$$I_{illum} = I_{ph} + I_{dark} = I_{dark}\left(\frac{P_{light}}{P_{light}^{S}} + 1\right)^{m} \quad (2)$$

As shown in Figure 5a, I_{illum} of the suspended and nonsuspended devices are plotted as a function of P_{light}. Since the two devices are both predominant by the Schottky junction, their I_{illum} can be well fitted with eq 2. From the fitting results, the P_{light}^{S} of the suspended and nonsuspended devices are 1.08×10^{-5} and 2.85×10^{-5} mW/cm^2, respectively. According to the definition of $P_{light}^{S} = \frac{\hbar\omega n_i}{2\alpha\tau_0}$, the minority carrier recombination lifetime of the suspended MoS_2 is a few times shorter than that of the nonsuspended MoS_2. This result is consistent with the experimental data described above. The ideality factors are extracted as 0.90 and 0.70 for the suspended and nonsuspended devices, respectively. The near unity ideality factor of the suspended device shows it is more effective to reduce the Schottky barrier by light illumination than the nonsuspended device. To further prove this, I_{ph} of the suspended and nonsuspended devices are extracted and plotted as a function of P_{light} (Figure 5b). While the I_{ph} of the suspended device shows a near linear dependence on P_{light}, the I_{ph} of the nonsuspended device gradually saturates as the P_{light} increases from 0.24 to 20.6 mW/cm^2.

It is notable that the suspended device shows better stability of responsivity R ($R = I_{ph}/(A \times P_{light})$, A is the device area) with varying light intensity than the nonsuspended device. As shown in Figure 5c, the normalized responsivities R/R_0 (R_0 is the responsivity with an initial light intensity of ~0.18 mW/cm^2) of three suspended and three nonsuspended devices are plotted as a function of P_{light}. When the light intensity increases from 0.18 to 26.2 mW/cm^2, the R values of nonsuspended devices decrease to about 20% of the initial value, while those of suspended devices only decrease to about 80%. For nonsuspended devices, the photocurrent originates from the combination of light-induced Schottky barrier reduction and photogating, which makes its initial R larger than that of the

https://doi.org/10.1021/acsphotonics.5c00146
ACS Photonics 2025, 12, 2656−2663

suspended device (Figure S4), but photocurrent from photogating has an obvious decay with the increase of light intensity due to the gradually filled trap states in the channel, which is quite common for such devices. As shown in Figure S5, the linear dynamic range (LDR) of the suspended device is determined using two additional devices by measuring the photocurrents over a larger range of light intensities, which shows high linearity of photocurrent at different light intensities, and leads to the excellent LDR of 66 and 54 dB. We further measure the noise power spectral densities of these two devices and extract the detectivity of the suspended phototransistors (Figure S6).

In addition, low dark current is also crucial for low-noise photodetectors.[34] However, it is generally difficult to simultaneously achieve a high response speed and low dark current. In Figure 5d, we summarize the dark current and response time (rise time) of photodetectors based on a pure MoS_2 channel.[7,17,35−38] The closer the data point is to the origin (lower left corner) of the coordinate axis, the better the device performance is. For the nonsuspended device in this work, it has a few seconds of response time and a relatively large dark current, making it far from ideal. For the suspended device, due to the existence of Schottky barrier and the separation of the MoS_2 channel oxide, it has very fast response speed (68.6 μs) and extremely low dark current (12 pA), which makes it closer to the origin than other reported devices and shows excellent performance.

While 2D heterojunction photodiodes also show high speed,[39−42] suspended 2D phototransistors support gate tuning of photodetection performance such as the photoresponsivity. As shown in Figure S7, by varying gate voltage, the responsivity can be tuned from 1.4×10^{-2} to 20.9 A/W, by more than 3 orders of magnitude at a light intensity of 2.6 mW/cm^2. Furthermore, the responsivity reaches 138.4 A/W at 0.21 mW/cm^2, which is much higher than that for 2D heterojunction photodiodes. The results show that the suspended phototransistor has the potential to achieve both high responsivity and high speed. Furthermore, the fully suspended structure allows us to reveal the intrinsic photoresponses of the 2D phototransistor without the substrate effect. The performance of the suspended 2D photodetectors can serve as a benchmark for interface-engineered 2D photodetectors.

CONCLUSION

In summary, photodetectors with high response speed and stable responsivity are prepared based on fully suspended 2D MoS_2. Due to the complete separation of the MoS_2 channel and Si substrate underneath, the photogating effect is effectively suppressed in this device. Then the photocurrent rise time and fall time are measured as 68.6 and 100.0 μs by transient photocurrent measurement, respectively, which are about 10^5 times faster than the nonsuspended devices. Moreover, the suspended devices exhibit stable responsivity within a large range of light intensity, which shows great potential for practical applications in photodetectors. A detailed analysis of the photoresponse mechanisms of MoS_2-based photodetectors is performed by designing devices with different structures and comparing their photoresponses. The results in this work can provide a fundamental understanding of photoresponse mechanisms of MoS_2-based photodetectors and guide the design of high-performance 2D photodetectors.

ASSOCIATED CONTENT

Supporting Information

The Supporting Information is available free of charge at https://pubs.acs.org/doi/10.1021/acsphotonics.5c00146.

Fabrication and measurement of suspended and nonsuspended MoS_2 photodetectors, basic $I-V$ characteristics without light illumination, cutoff frequency measurement, LDR measurement, noise measurement, gate tuning of responsivity, and measured responsivity at varying light intensity (PDF)

AUTHOR INFORMATION

Corresponding Authors

Yaping Dan − *University of Michigan − Shanghai Jiao Tong University Joint Institute, Shanghai Jiao Tong University, Shanghai 200240, China; State Key Laboratory of Advanced Optical Communication Systems and Networks, University of Michigan − Shanghai Jiao Tong University Joint Institute, Shanghai Jiao Tong University, Shanghai 200240, China;* orcid.org/0000-0002-2983-7213; Email: Yaping.dan@sjtu.edu.cn

Rui Yang − *University of Michigan − Shanghai Jiao Tong University Joint Institute, Shanghai Jiao Tong University, Shanghai 200240, China; State Key Laboratory of Radio Frequency Heterogeneous Integration, Shanghai Jiao Tong University, Shanghai 200240, China;* orcid.org/0000-0002-6163-2904; Email: rui.yang@sjtu.edu.cn

Authors

Jianyong Wei − *University of Michigan − Shanghai Jiao Tong University Joint Institute, Shanghai Jiao Tong University, Shanghai 200240, China*

Zhentao Lian − *University of Michigan − Shanghai Jiao Tong University Joint Institute, Shanghai Jiao Tong University, Shanghai 200240, China*

Yumeng Liu − *University of Michigan − Shanghai Jiao Tong University Joint Institute, Shanghai Jiao Tong University, Shanghai 200240, China*

Maosong Xie − *University of Michigan − Shanghai Jiao Tong University Joint Institute, Shanghai Jiao Tong University, Shanghai 200240, China*

Yueyang Jia − *University of Michigan − Shanghai Jiao Tong University Joint Institute, Shanghai Jiao Tong University, Shanghai 200240, China*

Kai Li − *University of Michigan − Shanghai Jiao Tong University Joint Institute, Shanghai Jiao Tong University, Shanghai 200240, China*

Robert Kudrawiec − *Department of Semiconductor Materials Engineering, Wroclaw University of Science and Technology, Wroclaw 50-370, Poland;* orcid.org/0000-0003-2593-9172

Complete contact information is available at: https://pubs.acs.org/10.1021/acsphotonics.5c00146

Author Contributions

⊥J.W. and Z.L. made an equal contribution.

Funding

This work was financially supported by the Oceanic Interdisciplinary Program of Shanghai Jiao Tong University (No. SL2022ZD107), the Shanghai Jiao Tong University Scientific and Technological Innovation Funds (No. 2020QY05), National Natural Science Foundation of China

(NSFC) (Grants 92364107, 62104140, U21A20505), Science and Technology Commission of Shanghai Municipality (STCSM) (Grants 23QA1405300, 24ZR1491500), Lingang Laboratory Open Research Fund (Grant LG-QS-202202−11), State Key Laboratory of Radio Frequency Heterogeneous Integration (Shenzhen University), Natural Science Foundation of Chongqing (CSTB2022NSCQ-MSX1095), and the Shanghai Pujiang Program (No. 22PJ1408200).

Notes

The authors declare no competing financial interest.

■ ACKNOWLEDGMENTS

The authors thank the Center for Advanced Electronic Materials and Devices (AEMD) for the support in device fabrication and characterization.

■ REFERENCES

(1) Wang, Q. H.; Kalantar-Zadeh, K.; Kis, A.; Coleman, J. N.; Strano, M. S. Electronics and optoelectronics of two-dimensional transition metal dichalcogenides. *Nat. Nanotechnol.* **2012**, *7* (11), 699−712.

(2) Zhang, W.; Huang, J. K.; Chen, C. H.; Chang, Y. H.; Cheng, Y. J.; Li, L. J. High-Gain Phototransistors Based on a CVD MoS_2 Monolayer. *Adv. Mater.* **2013**, *25* (25), 3456−3461.

(3) Shen, C.; Liu, Y.; Wu, J.; Xu, C.; Cui, D.; Li, Z.; Liu, Q.; Li, Y.; Wang, Y.; Cao, X.; et al. Tellurene Photodetector with High Gain and Wide Bandwidth. *ACS Nano* **2020**, *14* (1), 303−310.

(4) Xia, Y.; Chen, X.; Wei, J.; Wang, S.; Chen, S.; Wu, S.; Ji, M.; Sun, Z.; Xu, Z.; Bao, W.; et al. 12-in. growth of uniform MoS_2 monolayer for integrated circuit manufacture. *Nat. Mater.* **2023**, *22* (11), 1324−1331.

(5) Liu, Z.; Gong, X.; Cheng, J.; Shao, L.; Wang, C.; Jiang, J.; Cheng, R.; He, J. Wafer-scale synthesis of two-dimensional materials for integrated electronics. *Chip* **2024**, *3* (1), 100080.

(6) Radisavljevic, B.; Radenovic, A.; Brivio, J.; Giacometti, V.; Kis, A. Single-layer MoS_2 transistors. *Nat. Nanotechnol.* **2011**, *6* (3), 147−150.

(7) Lopez-Sanchez, O.; Lembke, D.; Kayci, M.; Radenovic, A.; Kis, A. Ultrasensitive photodetectors based on monolayer MoS_2. *Nat. Nanotechnol.* **2013**, *8* (7), 497−501.

(8) Hu, T.; Zhang, R.; Li, J.-P.; Cao, J.-Y.; Qiu, F. Photodetectors based on two-dimensional MoS_2 and its assembled heterostructures. *Chip* **2022**, *1* (3), 100017.

(9) Choi, W.; Cho, M. Y.; Konar, A.; Lee, J. H.; Cha, G. B.; Hong, S. C.; Kim, S.; Kim, J.; Jena, D.; Joo, J.; et al. High-Detectivity Multilayer MoS_2 Phototransistors with Spectral Response from Ultraviolet to Infrared. *Adv. Mater.* **2012**, *24* (43), 5832−5836.

(10) Sun, Y.; Jiang, L.; Wang, Z.; Hou, Z.; Dai, L.; Wang, Y.; Zhao, J.; Xie, Y.-H.; Zhao, L.; Jiang, Z.; et al. Multiwavelength High-Detectivity MoS_2 Photodetectors with Schottky Contacts. *ACS Nano* **2022**, *16* (12), 20272−20280.

(11) Liu, Y.; Weiss, N. O.; Duan, X.; Cheng, H.-C.; Huang, Y.; Duan, X. van der Waals heterostructures and devices. *Nat. Rev. Mater.* **2016**, *1* (9), 16042.

(12) Ma, Y.; Li, Y.; Wang, H.; Wang, M.; Wang, J. High performance flexible photodetector based on 0D-2D perovskite heterostructure. *Chip* **2023**, *2* (1), 100032.

(13) Abbas, K.; Ji, P.; Ullah, N.; Shafique, S.; Zhang, Z.; Ameer, M. F.; Qin, S.; Yang, S. Graphene photodetectors integrated with silicon and perovskite quantum dots. *Microsyst. Nanoeng.* **2024**, *10* (1), 81.

(14) Lian, Z.; Wei, J.; Liu, Z.; Chen, G.; Kuo, H.-C.; Dan, Y.; Tu, C.-C.; Yang, R. High-Detectivity UV-Sensitive 2D MoS_2 Phototransistors Enhanced by Silicon Quantum Dots. *ACS Photonics* **2024**, *11* (10), 4224−4234.

(15) Kwon, J.; Hong, Y. K.; Han, G.; Omkaram, I.; Choi, W.; Kim, S.; Yoon, Y. Giant Photoamplification in Indirect-Bandgap Multilayer MoS_2 Phototransistors with Local Bottom-Gate Structures. *Adv. Mater.* **2015**, *27* (13), 2224−2230.

(16) Kufer, D.; Konstantatos, G. Highly Sensitive, Encapsulated MoS_2 Photodetector with Gate Controllable Gain and Speed. *Nano Lett.* **2015**, *15* (11), 7307−7313.

(17) Huang, Y.; Zhuge, F.; Hou, J.; Lv, L.; Luo, P.; Zhou, N.; Gan, L.; Zhai, T. Van der Waals Coupled Organic Molecules with Monolayer MoS_2 for Fast Response Photodetectors with Gate-Tunable Responsivity. *ACS Nano* **2018**, *12* (4), 4062−4073.

(18) Fang, H.; Hu, W. Photogating in Low Dimensional Photodetectors. *Adv. Sci.* **2017**, *4* (12), 1700323.

(19) Island, J. O.; Blanter, S. I.; Buscema, M.; van der Zant, H. S. J.; Castellanos-Gomez, A. Gate Controlled Photocurrent Generation Mechanisms in High-Gain In_2Se_3 Phototransistors. *Nano Lett.* **2015**, *15* (12), 7853−7858.

(20) Illarionov, Y. Y.; Rzepa, G.; Waltl, M.; Knobloch, T.; Grill, A.; Furchi, M. M.; Mueller, T.; Grasser, T. The role of charge trapping in MoS_2/SiO_2 and MoS_2/hBN field-effect transistors. *2D Mater.* **2016**, *3* (3), 035004.

(21) Jadczak, J.; Kutrowska-Girzycka, J.; Bieniek, M.; Kazimierczuk, T.; Kossacki, P.; Schindler, J. J.; Debus, J.; Watanabe, K.; Taniguchi, T.; Ho, C. H.; et al. Probing negatively charged and neutral excitons in MoS_2/hBN and hBN/MoS_2/hBN van der Waals heterostructures. *Nanotechnology* **2021**, *32* (14), 145717.

(22) Lee, C.; Rathi, S.; Khan, M. A.; Lim, D.; Kim, Y.; Yun, S. J.; Youn, D.-H.; Watanabe, K.; Taniguchi, T.; Kim, G.-H. Comparison of trapped charges and hysteresis behavior in hBN encapsulated single MoS_2 flake based field effect transistors on SiO_2 and hBN substrates. *Nanotechnology* **2018**, *29* (33), 335202.

(23) Yang, R.; Zheng, X.; Wang, Z.; Miller, C. J.; Feng, P. X. L. Multilayer MoS_2 transistors enabled by a facile dry-transfer technique and thermal annealing. *J. Vac. Sci. Technol. B* **2014**, *32* (6), 061203.

(24) Lee, C.; Yan, H.; Brus, L. E.; Heinz, T. F.; Hone, J.; Ryu, S. Anomalous Lattice Vibrations of Single- and Few-Layer MoS_2. *ACS Nano* **2010**, *4* (5), 2695−2700.

(25) Di Bartolomeo, A.; Grillo, A.; Urban, F.; Iemmo, L.; Giubileo, F.; Luongo, G.; Amato, G.; Croin, L.; Sun, L.; Liang, S. J.; et al. Asymmetric Schottky Contacts in Bilayer MoS_2 Field Effect Transistors. *Adv. Funct. Mater.* **2018**, *28* (28), 1800657.

(26) Ezhilmaran, B.; Patra, A.; Benny, S.; Sreelakshmi, M. R.; Akshay, V. V.; Bhat, S. V.; Rout, C. S. Recent developments in the photodetector applications of Schottky diodes based on 2D materials. *J. Mater. Chem. C* **2021**, *9* (19), 6122−6150.

(27) Liu, X.; Choi, M. S.; Hwang, E.; Yoo, W. J.; Sun, J. Fermi Level Pinning Dependent 2D Semiconductor Devices: Challenges and Prospects. *Adv. Mater.* **2022**, *34* (15), 2108425.

(28) Pak, S.; Lee, J.; Jang, A. R.; Kim, S.; Park, K. H.; Sohn, J. I.; Cha, S. Strain-Engineering of Contact Energy Barriers and Photoresponse Behaviors in Monolayer MoS_2 Flexible Devices. *Adv. Funct. Mater.* **2020**, *30* (43), 2002023.

(29) Kwon, S.; Kwon, M. H.; Song, J.; Kim, E.; Kim, Y.; Kim, B. R.; Hyun, J. K.; Lee, S. W.; Kim, D.-W. Light-Induced Surface Potential Modification in MoS_2 Monolayers on Au Nanostripe Arrays. *Sci. Rep.* **2019**, *9* (1), 14434.

(30) Jiang, J.; Wen, Y.; Wang, H.; Yin, L.; Cheng, R.; Liu, C.; Feng, L.; He, J. Recent Advances in 2D Materials for Photodetectors. *Adv. Electron. Mater.* **2021**, *7* (7), 2001125.

(31) Long, M.; Wang, P.; Fang, H.; Hu, W. Progress, Challenges, and Opportunities for 2D Material Based Photodetectors. *Adv. Funct. Mater.* **2018**, *29* (19), 1803807.

(32) Khaleghi, S. S. M.; Wei, J.; Crozier, K. B.; Dan, Y. *High-Performance MoS_2 Photodetectors by Photogating*; Conference on Lasers and Electro-Optics Pacific Rim (CLEO-PR), 2024; pp P3-043.

(33) Wei, J.; Liu, Y.; Wang, Y.; Li, K.; Lian, Z.; Xie, M.; Yang, X.; Khaleghi, S. S. M.; Dai, F.; Hu, W.; Gao, X.; Yang, R.; Dan, Y. Analytical photoresponses of Schottky contact MoS_2 phototransistors. *Small* **2024**, *21*, 2408508.

(34) Taffelli, A.; Dirè, S.; Quaranta, A.; Pancheri, L. MoS_2 Based Photodetectors: A Review. *Sensors* **2021**, *21* (8), 2758.

https://doi.org/10.1021/acsphotonics.5c00146
ACS Photonics 2025, 12, 2656−2663

(35) Gant, P.; Huang, P.; Pérez de Lara, D.; Guo, D.; Frisenda, R.; Castellanos-Gomez, A. A strain tunable single-layer MoS_2 photodetector. *Mater. Today* **2019**, *27*, 8−13.
(36) Zhang, X.-L.; Li, J.; Leng, B.; Yang, L.; Song, Y.-D.; Feng, S.-Y.; Feng, L.-Z.; Liu, Z.-T.; Fu, Z.-W.; Jiang, X.; et al. High-performance ultraviolet-visible photodetector with high sensitivity and fast response speed based on MoS_2-on-ZnO photogating heterojunction. *Tungsten* **2023**, *5* (1), 91−99.
(37) Tsai, D. S.; Liu, K. K.; Lien, D. H.; Tsai, M. L.; Kang, C. F.; Lin, C. A.; Li, L. J.; He, J. H. Few-Layer MoS_2 with High Broadband Photogain and Fast Optical Switching for Use in Harsh Environments. *ACS Nano* **2013**, *7* (5), 3905−3911.
(38) Zhang, X.-M.; Tseng, S.-H.; Lu, M.-Y. Large-Area Ultraviolet Photodetectors Based on p-Type Multilayer MoS_2 Enabled by Plasma Doping. *Appl. Sci.* **2019**, *9* (6), 1110.
(39) Ye, L.; Wang, P.; Luo, W.; Gong, F.; Liao, L.; Liu, T.; Tong, L.; Zang, J.; Xu, J.; Hu, W. Highly polarization sensitive infrared photodetector based on black phosphorus-on-WSe_2 photogate vertical heterostructure. *Nano Energy* **2017**, *37*, 53−60.
(40) Li, F.; Xu, B.; Yang, W.; Qi, Z.; Ma, C.; Wang, Y.; Zhang, X.; Luo, Z.; Liang, D.; Li, D.; Li, Z.; Pan, A. High-performance optoelectronic devices based on van der Waals vertical MoS_2/$MoSe_2$ heterostructures. *Nano Res.* **2020**, *13*, 1053−1059.
(41) Shin, G. K.; Park, C.; Lee, K. J.; Jin, H. K.; Choi, S. Y. Ultrasensitive phototransistor based on WSe_2−MoS_2 van der Waals heterojunction. *Nano Lett.* **2020**, *20* (8), 5741−5748.
(42) Long, M.; Liu, E.; Wang, P.; Gao, A.; Xia, H.; Luo, W.; Wang, B.; Zeng, J.; Fu, Y.; Xu, K.; Zhou, W.; Lv, Y.; Yao, S.; Lu, M.; Chen, Y.; Ni, Z.; You, Y.; Zhang, X.; Qin, S.; Shi, Y.; Hu, W.; Xing, D.; Miao, F. Broadband photovoltaic detectors based on an atomically thin heterostructure. *Nano Lett.* **2016**, *16*, 2254−2259.

https://doi.org/10.1021/acsphotonics.5c00146
ACS Photonics 2025, 12, 2656−2663